ADVANCED OPTICAL MATERIALS
www.advopticalmat.de

From Blue to White: Sustainable Luminescent Metal Organic Framework for Hybrid Light-Emitting Diodes

Youssef Atoini, Luca M. Cavinato, Julio Fernandez-Cestau, Yvonne Gmach, Daniel Van Opdenbosch, and Rubén D. Costa**

Hybrid light-emitting diodes based on photon down-converting filters with metal organic frameworks (MOFs) are mainly restricted to cross-breed materials (i.e., nonemissive MOFs host and guest emitters) due to the lack of highly photostable and luminescent MOFs (LMOFs). This work reports a sustainable and cost-effective blue-emitting Zn-based MOF with the ligand 1,1,2,2-tetrakis(4-(pyridin-4-yl)phenyl)ethene (Zn-2-LMOF) and their host:guest hybrids with Rhodamine B emitter RhB@LMOF toward blue- and white-emitting hybrid light-emitting diodes (HLEDs). Zn-2-LMOF features blue emission (λ_{em} = 480 nm) with impressive photoluminescence quantum yield (ϕ) values of 50% (powder) and 70% (polystyrene coatings). Likewise, hybrid RhB@LMOF features a white emission with ϕ of 30–40% in polystyrene coatings. They lead to blue (Zn-2-LMOF; *x/y* CIE color coordinates of 0.28/0.47) and white (RhB@LMOF; *x/y* CIE color coordinates of 0.31/0.32) HLEDs with stabilities of 20 and 45 h at 50 mA on-chip under ambient operation, respectively. Though this device performance is average in HLEDs, the device degradation is mainly attributed to the photoinduced oxidation of the ligand in the MOF structure that further leads to the RhB degradation; a key information for future developments in luminescent MOFs.

1. Introduction

White light-emitting diodes (WLEDs) consist of a UV-/blue-emitting inorganic chip coated by a photon-down-converting filter, more commonly called phosphor.[1] This coating partially converts the high-energy emission into a broad low-energy emission band, leading to an overall white emission with excellent color rendering index (CRI) and correlated color temperature (CCT), while device stability and efficiency strongly depend on the type of phosphor. On the one hand, commercial WLEDs use inorganic phosphors (IPs) based on either rare-earth,[2] such as Ce^{3+} or Eu^{2+} doped yttrium-aluminium garnet ($Y_3Al_5O_{12}$; YAG), or toxic cadmium selenides quantum dots (Cd/Se QDs).[3] Although they meet the customer requirements in terms of color quality and device performance, their critical environmental impact (mining, transport, and toxicity) and very high cost (purification and recycling) mandate the search of more sustainable and cost-effective photon down-converting filters. On the other hand, organic phosphors (OPs) have experienced a strong development in the so-called hybrid light-emitting diodes (HLEDs)[4] as a real alternative toward the next generation of LED lighting sources. They are based on conjugated polymers,[5] coordination complexes,[6] organic dyes,[7] or fluorescent proteins[4] embedded into polymer/epoxy coatings. While excellent white color quality has been achieved, the main issue consists of device stability at high luminous efficiencies. To date, average values are stabilities of a few hours at efficiencies <30 lm W^{-1},[4–7] while the best performing HLEDs are based on OPs with perylene diimide (<700 h at ≈100 lm W^{-1}),[8] Ir(III) complexes[9] (<1000 h at ≈100 lm W^{-1}) and fluorescent protein (<3500 h at ≈130 lm W^{-1}).[10] In most cases, the luminescent features of the OPs are compromised upon coating fabrication due to chemical degradation of the emitters and/or strong aggregation-induced emission quenching.[11] Thus, the stabilization of the emitter in polymer matrices is a critical aspect in HLEDs.

To overcome these benchmarks, the design of white-emitting host–guest hybrid materials, in which the guest (emitter) is stabilized by the host (i.e., a porous material, such as metal organic frameworks (MOFs), silica, and zeolites), has been explored.[9a,12] Among them, MOFs are of high interest due to their straightforward syntheses and postsynthetic modification, high degree of crystallinity, nanoscale processability, and predictable structures for large surface area and relatively tuneable porosity.[13] They consist of one or several metal ion center(s) (either metal ion(s) or cluster(s)), called node(s), bonded to one or several organic moiety(ies) called ligand(s) or linker(s). The

Y. Atoini, L. M. Cavinato, J. Fernandez-Cestau, R. D. Costa
Technical University of Munich
Chair of Biogenic Functional Materials
Schulgasse 22, 94315 Straubing, Germany
E-mail: y.atoini@tum.de; ruben.costa@tum.de
Y. Gmach, D. Van Opdenbosch
Chair for Biogenic Polymers
Schulgasse 16, 94315 Straubing, Germany
The ORCID identification number(s) for the author(s) of this article can be found under https://doi.org/10.1002/adom.202202643.

DOI: 10.1002/adom.202202643

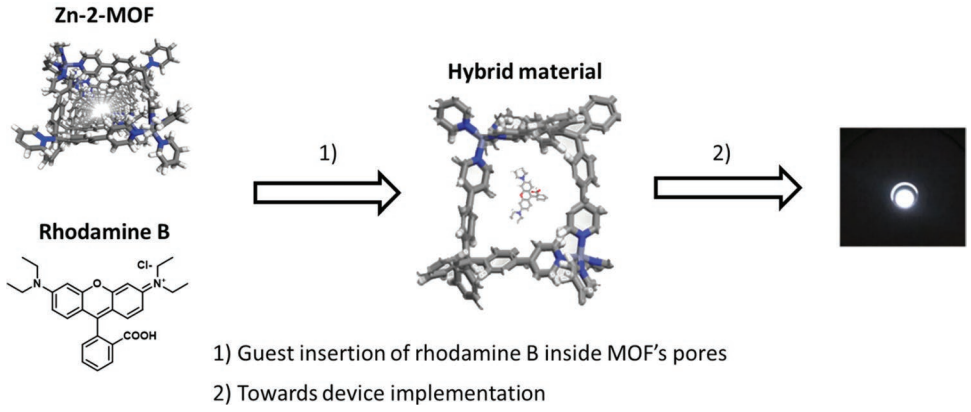

Figure 1. Work concept depicting the guest insertion of Rhodamine B inside LMOF (**Zn-2-LMOF)** to form the white-emitting hybrid material that is further used as a color filter in white hybrid light-emitting diodes (HLEDs; right picture).

repetition between the node(s) and the linker(s) forms a geometrically well-defined, highly crystalline, and porous structure. They are, indeed, widely investigated in gas separation,[14] gas storage,[14a-b,15] catalysis,[16] medicine,[17] etc. However, their applications in lighting systems still remain as a challenge as only roughly 15% of the reported MOFs are described as luminescent MOFs (LMOFs),[12] while, among them, only a few are interesting for artificial illumination due to their relatively low ϕ,[12c,18] lack of sustainability,[19] and hard implementation.[20,21] As the best example, Li an co-workers reported one of the pioneer white-emitting LMOF-HLED using a blue-emitting Cd-based LMOF as a host of yellow emissive Ir(III) complex and orange/red emissive rare-earth emitters.[18] The white hybrid LMOF featured $\phi = 20\%$, performing HLEDs with a high white quality (x/y CIE color coordinates of 0.31/0.33, CRI of 80, and CCT of 5900 K), but the device stability and efficiency were nondisclosed.

Taking into account this scenario, this work sets in a new approach toward designing blue-emitting sustainable and cost-effective Zn-based LMOFs and their white hybrid derivatives using Rhodamine (RhB) as guest emitter (**Figure 1**). On the one hand, we selected the ligand 1,1,2,2-tetrakis(4-(pyridin-4-yl) phenyl)ethene in concert with Zn^{2+} coordination moiety (Zn-2-MOF; Figure 1) due to its extended π-conjugation and the softness of the pyridine anchoring moiety, leading to highly efficient blue emission (λ_{em} = 480 nm) with ϕ values of 50% (powder) and 70% (OPs) that are among the highest reported LMOF—vide supra.[12c,18] On the other hand, the insertion of RhB into the porous structure (RhB@MOF; Figure 1) led to a white hybrid material featuring a broad whitish emission band peaking at 480 and 580 nm associated to ϕ values of 30–40% in OPs. As reference, the polymer coating with the same amount of RhB did not show any photoluminescent response as it is prone to agglomerate.[22] Finally, the interesting emission features of the above OPs led to blue/green (**Zn-2-LMOF**; x/y CIE color coordinates of 0.28/0.47) and white (**RhB@LMOF**; x/y CIE color coordinates of 0.31/0.32, CRI of 85, and CCT of 6835 K) HLEDs with average stabilities of 20 and 45 h, respectively. What is more, we rationalized that the degradation pathway mainly involves the photoinduced oxidation of the ligand in the MOF that promotes the photoinduced degradation of RhB; a key aspect to redesign more photostable LMOFs for lighting applications.

2. Results and Discussion

2.1. Synthesis and Characterization of Blue- and White-Emitting LMOFs and Their Respective OPs

The tetraphenylethylene derivative ligand **2** was synthesized according to a previous work[27] (**Scheme 1** and Experimental Section) and characterized by means of ^{1}H and ^{13}C nuclear magnetic resonance (NMR) and ESI high-resolution mass spectrometry (HRMS) (Figures S1–S4, Supporting Information). In short, the first step is a tetra bromination of 1,1,2,2-tetraphenylethene to obtain the intermediate **1**, while the second step is a Suzuki coupling to obtain **2**. Solvotermal reaction of $ZnCl_2$ and **2** in DMF was performed for the MOF synthesis (**Zn-2-LMOF**). The Soxhlet extraction in ethanol allows a replacement of DMF molecules inside the MOFs pores with ethanol molecules. Powder X-ray diffraction (PXRD) experiment followed

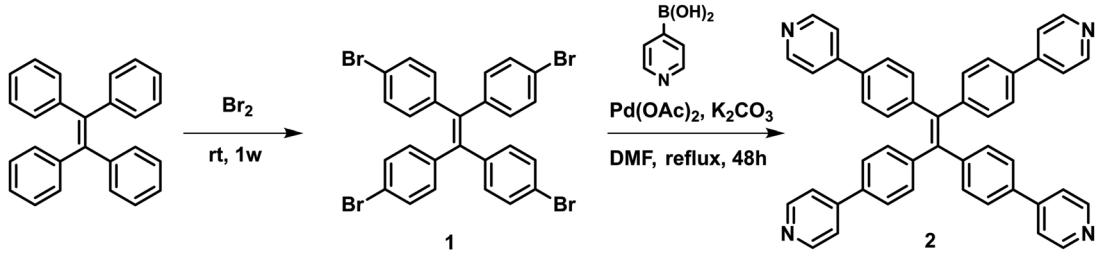

Scheme 1. Synthetic pathway of ligand **2**.

Table 1. Photophysical features of **Zn-2-LMOF** and **2** in powder and polystyrene (PS) matrix.

Sample	λ_{em} [nm]	FWHM [nm]	ϕ [%] (λ_{exc} = 370 nm)	τ [ns] (λ_{exc} = 370 nm)	k_r [s^{-1}]	k_{nr} [s^{-1}]
Zn-2-LMOF powder	482	81	53	2.98 (480 nm)	$1.78 \times 10^{[8]}$	$1.57 \times 10^{[8]}$
Zn-2-LMOF@PS	482	114	71	2.96 (480 nm)	$2.40 \times 10^{[8]}$	$9.8 \times 10^{[7]}$
2@PS	484	91	38	3.05 (480 nm)	$1.24 \times 10^{[8]}$	$2.03 \times 10^{[8]}$

by indexing and refinement reveals a monoclinic crystalline phase (space group: P12/m1; a = 25.95 Å, b = 7.33 Å, c = 24.18 Å; β = 94.17°; cf. Figure S5, Supporting Information). Scanning electron microscopy micrographs show that the **Zn-2-LMOF** forms large crystalline needles (Figure S6, Supporting Information). Finally, thermogravimetric analysis (Figure S7, Supporting Information) depicts a certain stability of the MOF up to 350 °C, in which more than 80% of the initial mass held. Above 360 °C, the MOF is not stable and a sudden drop of the mass is noted up to 500 °C; temperature at which 100% of the initial mass is lost. This sudden drop of mass is due to ligand degradation. Nitrogen adsorption–desorption experiments were conducted on the **Zn-2-MOF** (cf. Figure S8, Supporting Information) and reveal a surface area of 205 m^2 g^{-1} together with a pore diameter of 3.6 nm. The latter matches the length of ligand.

A summary of the photophysical properties of **2** and **Zn-2-LMOF** are gathered in **Table 1**, while **Figure 2** displays the excitation and emission spectra of **Zn-2-LMOF** in powder. The emission spectrum of **Zn-2-LMOF** in powder consists of a broad, featureless band centered at 480 nm (full width at half maximum (FWHM) of 81 nm) with a ϕ of 53% and an excited state lifetime (τ) of 2.98 ns (cf. Figure S9a, Supporting Information). This prompt us to conclude that the emission mechanism must be related to fluorescence process located at the bridged ligand and attributed to a ligand centered emission.[12c,28] This was further confirmed in self-standing and mm-thick OPs prepared with **2** and **Zn-2-LMOF** embedded into a polystyrene matrix (see Experimental Section). In detail, the emission spectrum of **Zn-2-LMOF@PS** slightly broadens without changing its emission maxima compared to that of powder, but the ϕ significantly increases up to values of 70% without affecting τ values (Table 1). As reference, **2@PS** features similar emission and excitation band shapes as well as τ values (Figure S10, Supporting Information and Table 1), while ϕ is almost half of the LMOF coating (i.e., 38%). This emphasizes the importance of the metal ion coordination, for both, rigidifying the ligand conformation and avoiding aggregation, leading to a less prominent nonradiative decay.[29]

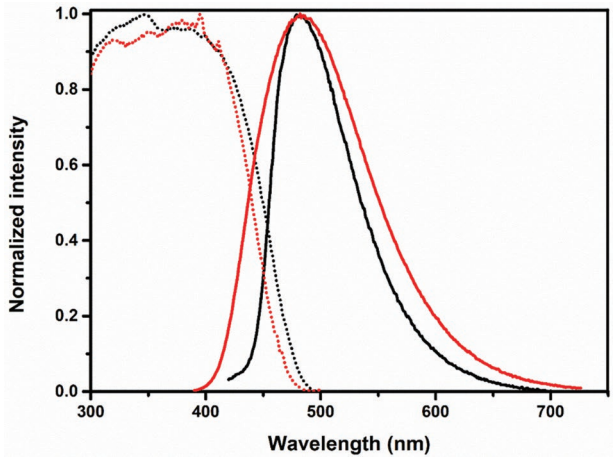

Figure 2. Excitation (dotted line, λ_{em} = 480 nm) and emission (full line, λ_{exc} = 370 nm) spectra of **Zn-2-LMOF** in powder (black line) and polystyrene (PS; red line) matrix.

The white emissive host–guest hybrid system was prepared by embedding the orange/reddish emitter RhB (guest) into the porous structure of the blue-emitting **Zn-2-LMOF** (host) as they feature complementary emission spectra and a matching overlap between the emission of the host and the absorption of the guest. This will allow an efficient energy transfer from the host to the guest—vide infra. In addition, the success of this approach will be easily attested by activating the emission of RhB, as it is well-known to be only emissive in solution as the emission is totally quenched in solid-state (powder and thin film).[30]

The insertion of RhB inside **Zn-2-LMOF** was carried out via solution transfer upon strong stirring over time by mixing different mass ratios of RhB:MOF, namely 10% (**RhB@LMOF-A**), 20% (**RhB@LMOF-B**), 40% (**RhB@LMOF-C**), 50% (**RhB@LMOF-D**), 100% (**RhB@LMOF-E**), and 200% (**RhB@LMOF-F**) (Figure S11, Supporting Information, for pictures of the samples). It is important to underline that the percentage does not refer to the loading ratio—vide infra, but to the amount employed at the beginning of the guest insertion reaction (Experimental Section and Table S1, Supporting Information, for details). The hybrid materials were washed with *n*-hexanol, since ethanol washing led to lower loading ratio and less contribution of the red emission. This is in line with the work of Calzaferri's group, who established that relatively long chain alcohols, such as *n*-butanol, are better washing agents than their short chain analogues, such as methanol or ethanol after guest insertion.[31] The guest loading was determined following two procedures (see Experimental Section and Table S1, Supporting Information, for details). At first, the supernatants from all the samples were collected and the solvent was evaporated under high vacuum (10^{-2} mbar). Knowing i) the amount of RhB employed at the beginning at the guest insertion process, and ii) that the supernatant resulting from the numerous washing/centrifuging experiments was no longer colorful, the amount of RhB remaining in the pores can be calculated by a simple subtraction. As a second procedure, dry samples were rediluted in methanol and their absorption features were measured (Figure S12, Supporting Information). Given the molar extinction coefficient of RhB in methanol or ethanol (106 000 cm^{-1} M^{-1}),[32] the amount of RhB was determined. Both

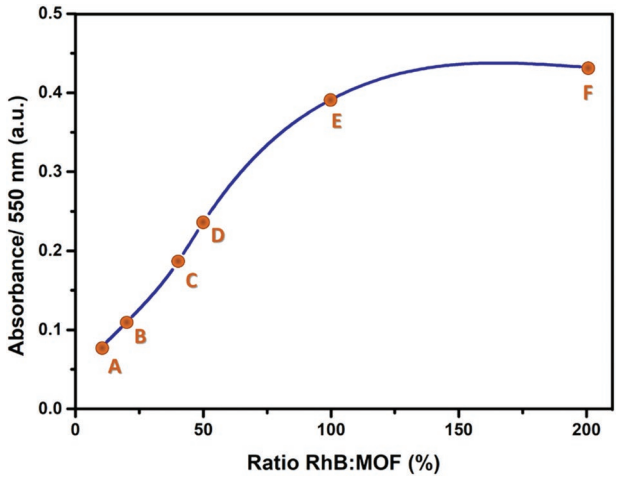

Figure 3. Absorbance at 550 nm of the RhB supernatant versus initial amount employed of RhB in the guest insertion process.

methods confirmed that the amount of RhB inside the LMOF spans between 0.060 and 1.778 mg mg^{-1} of ratio RhB:LMOF. As expected, the final host:guest mass ratio is not proportional to the initial host:guest ratio (**Figure 3**). The increase of the initial amount of RhB leads to a linear loading rise of RhB reaching, a 12-fold increase by comparing **RhB@LMOF-A** and **RhB@LMOF-E**, while this barely changes between **RhB@LMOF-E** and **RhB@LMOF-F**. Finally, all the above **RhB@LMOF** samples exhibit the same X-ray pattern of a triclinic crystal system (Figure S13, Supporting Information, P-1; a = 8.08 Å; b = 17.08 Å; c = 18.60 Å; α = 94.18°; β = 94.07°; γ = 96.27°), but slightly differ from that of the **Zn-2-LMOF**—vide supra. This further confirms the encapsulation of the RhB inside the MOF structure, as the guest may modify the arrangement of the MOF.[33] The encapsulation phenomenon was also confirmed by means of nitrogen adsorption–desorption measurements of **RhB@LMOF** sample, from which the pore diameter and the surface area were found as 6.6 m^2 g^{-1} and 3.8 nm, respectively. While the latter value is in the range of that of the neat MOF—vide supra—one can observe signals in the region of smaller pores. Moreover, the surface area shows a value smaller than that of the neat MOF, indicating the presence of filled pores (cf. Figure S14, Supporting Information). These data clearly emphasize the presence of the guest inside the host.

As for the neat Zn-2-LMOF, these samples were embedded into the polystyrene polymer coatings (**RhB@LMOF@PS**) to study the photoluminescent features of the OPs (see Experimental Section). At exclusively excitation of the LMOF moiety (λ_{exc} = 370 nm), the emission spectra (**Figure 4** and Figure S15, Supporting Information) depict, for all the samples, dual emissions consisting of two broad, featureless bands located at 480 nm (**Zn-2-LMOF**) and 580 nm (**RhB**). This indicates the absence of RhB aggregation due to the "dilution effect" into the MOF structure and an effective energy transfer process from the host to the guest. This is supported by the analysis of the excitation spectra (Figure S16, Supporting Information) and the τ values (**Table 2**). Firstly, the excitation spectra of the RhB in the **RhB@LMOF** include the absorption features related to the **Zn-2-LMOF**. Secondly, while the τ of **Zn-2-LMOF** moiety

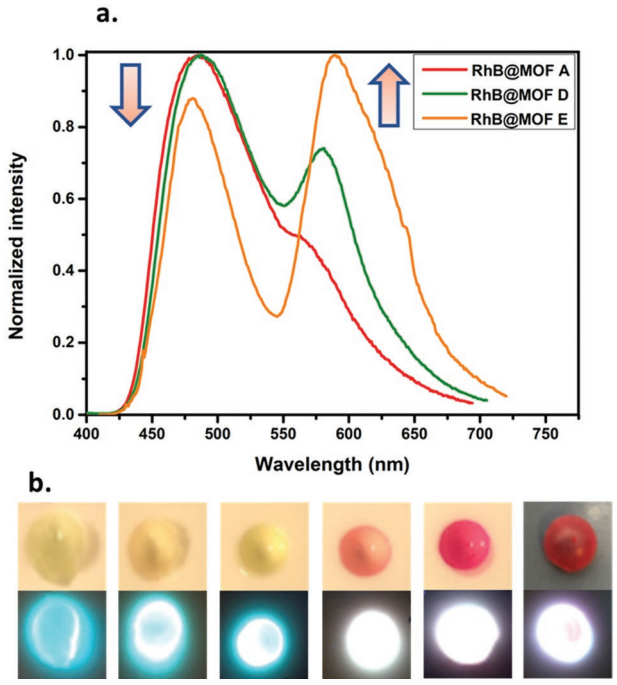

Figure 4. a) Emission spectra of an exemplary of **RhB@LMOF@PS** (λ_{exc} = 370 nm), highlighting the increase of the RhB emission intensity with the increase of the RhB load. b) Pictures of the samples under ambient light (top) and under UV lamp excitation (365 nm). From left to right: **Zn-2-LMOF**, **RhB@LMOF-A**, **RhB@MOF-B**, **RhB@LMOF-C**, **RhB@LMOF-D**, **RhB@LMOF-E**, and **RhB@LMOF-F**.

emission corresponds to a biexponential decay (Table 2, Figure S9b, Supporting Information), in which the higher energy component is half of that of the τ of the neat LMOF (1.4 vs. 2.9 ns) and the lower energy component corresponds to that of the RhB moiety (3.6 ns). Finally, the relative intensity between these peaks is nicely controlled by the **RhB** loading into the LMOF structure, reaching a white emission as shown in Figure 4. In addition, these OPs still retain a high ϕ of 30–40% (Table 2), highlighting their potential for HLEDs—vide supra.

2.2. Fabrication and Characterization of Hybrid Light-Emitting Diodes

HLEDs were fabricated using a 380 nm LED chip covered with either **Zn-2-LMOF@PS** or **RhB@LMOF-E@PS** coatings using an on-chip configuration (Figure S17, Supporting Information, and **Figure 5**, respectively; see Experimental Section for details). At different applied currents, the conversion of the **Zn-2-LMOF@PS** is almost complete, featuring a broad and featureless emission centered at 480 nm and a maximum luminous efficiency of ≈35 lm W^{-1} at the applied current regime of 20–50 mA (Figure S17, Supporting Information). Next, the device stability was investigated under ambient conditions at 50 mA that corresponds to the peak efficiency. Here, the emission of the **Zn-2-LMOF@PS** coating exponentially decreases, reaching lifetime values of $t_{0.5}$ = ≈20 h (i.e., time to reach half of the initial emission intensity). This decrease is exclusively related to photoinduced degradation, as the temperature of

Table 2. Photophysical features of **Zn-2-LMOF** and the hybrid materials in polystyrene (PS) matrix.

Sample	λ_{em} [nm]	FWHM [nm]	ϕ [%] (λ_{exc} = 370 nm)	τ [ns] (λ_{exc} = 370 nm)	k_r [$s^{-1} \times 10^8$]	k_{nr} [$s^{-1} \times 10^8$]
2	488	95	33	3.23 (488 nm)	1.02	2.07
Zn-2-LMOF	482	80	71	2.96 (482 nm)	2.40	0.98
RhB@LMOF-A	484, 578 (sh*)	n.d.**	50	1.5 (484 nm); 3.1 (578 nm)	3.3 (484 nm); 1.6 (578 nm)	3.3 (484 nm); 1.6 (578 nm)
RhB@LMOF-B	482, 578 (sh*)	n.d.**	48	1.5 (482 nm); 3.6 (578 nm)	3.2 (482 nm); 1.5 (578 nm)	3.5 (482 nm); 1.7 (578 nm)
RhB@LMOF-C	484, 582	n.d.**	41	1.5 (484 nm); 3.4 (582 nm)	2.7 (484 nm); 1.2 (582 nm)	3.9 (484 nm); 1.7 (582 nm)
RhB@LMOF-D	486, 581	n.d.**	38	1.4 (486 nm); 3.3 (581 nm)	2.7 (486 nm); 1.1 (581 nm)	4.1 (486 nm); 1.9 (581 nm)
RhB@LMOF-E	481, 588	60 (480 nm); 83 (580 nm)	33	1.3 (481 nm); 3.2 (588 nm)	2.5 (481 nm); 1.0 (588 nm)	5.1 (481 nm); 2.1 (588 nm)
RhB@LMOF-F	477, 584	43 (480 nm); 68 (580 nm)	31	1.1 (477 nm); 3.2 (584 nm)	2.8 (477 nm); 1.0 (584 nm)	6.3 (477 nm); 2.1 (584 nm)

*sh = shoulder, **n.d. = not determined.

the coating remains constant at around 30 °C. As first hint to elucidate the degradation mechanism is noted by the progressive red-shift of the emission maxima to ≈550 nm, suggesting the photooxidation of **2** into hydroxypyridine derivatives.[34] In order to corroborate this statement, HLEDs with **2@PS** were prepared and driven at the same conditions. As shown in Figure S18 (Supporting Information), the t_{50} values only reaches 2.5 h, while the emission spectrum also progressively red-shifts. Both findings confirm that the metal ion coordination in the LMOF not only increases the ϕ in polymer coatings—vide supra, but it also slows down the photoinduced oxidations of the ligand.

Likewise, the HLEDs prepared with **RhB@LMOF-E@PS** featured an almost complete conversion with a white electroluminescent spectrum (Figure 5) and a maximum luminous efficiency of 1.4 lm W^{-1} at the applied current regime of 20–50 mA.

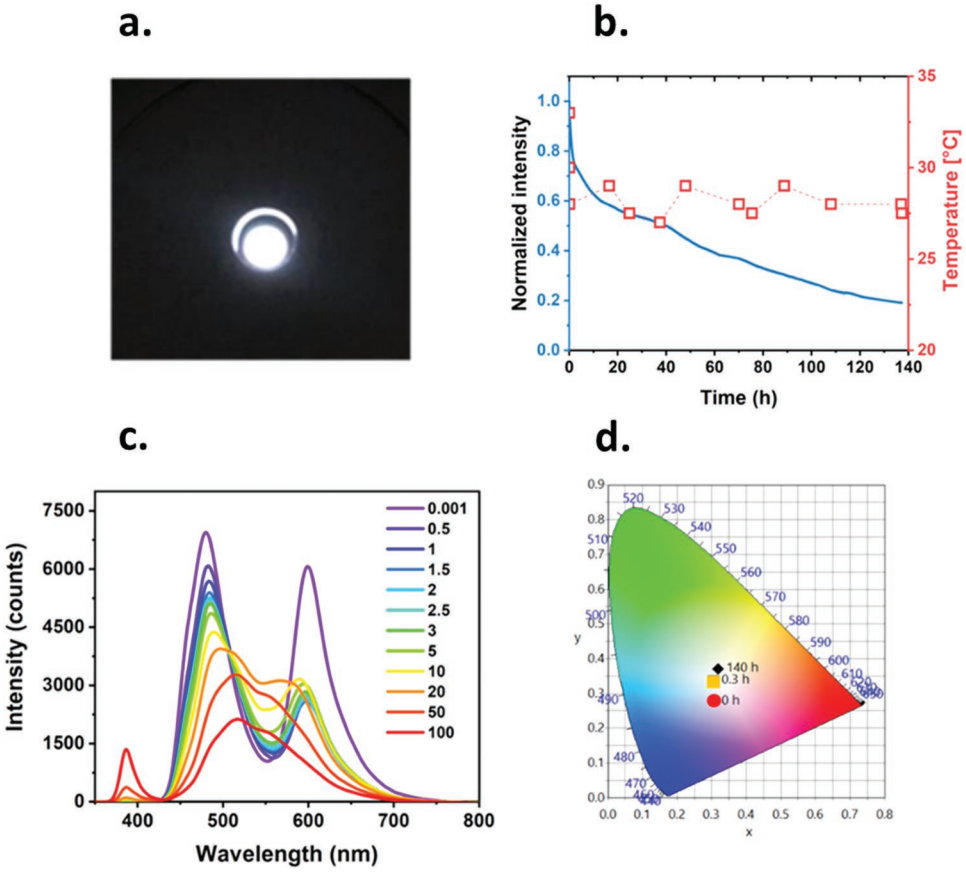

Figure 5. Top: a) Picture and b) emission intensity and temperature changes of the coatings of on-chip hybrid light-emitting diode (HLED) with **RhB@LMOF-E@PS**. Bottom: c) electroluminescent spectra over time (caption: time given in hours) d) and their corresponding *x*/*y* CIE color coordinates of the on-chip HLED with **RhB@LMOF-E@PS** at constant 50 mA under ambient conditions along time. Red circle = t_0, orange square = 20 min, black rhombus = 140 h.

Similar to the **Zn-2-LMOF**-HLED, the device stability at 50 mA under ambient conditions is characterized by an initial exponential decay over the **Zn-2-LMOF** emission band is noted over the first 15–20 h (Figure 5), while the RhB emission holds constant. At this point, both emission bands collapse and reduce linearly intensity, reaching a t_{50} of 45 h. Thus, we can conclude that the **Zn-2-LMOF** effectively protects the RhB emission, while its degradative product promotes the slow photodegradation of the RhB. As far as the chromaticity is concerned, a white emission with x/y CIE coordinates of 0.31/0.32, CCT of 6835 K, and CRI of 85 is noted for the first period changing to a final whitish emission that corresponds to x/y CIE color coordinates of 0.32/0.35, CCT of 6023 K, and CRI of 80. In order to enhance the stability of HLEDs with **RhB@LMOF-E@PS**, the devices were fabricated with a remote configuration (i.e., placing the photon down-converting coating at a distance of 2 cm from the LED chip). While the emission decay profile is similar to that of on-chip devices, the device lifetime is improved to 75 h (**Figure 6**), holding white emission quality going from initial x/y CIE = 0.30/0.28; CCT = 7900 K; CRI = 70 to x/y CIE = 0.31/0.33; CCT = 7200 K; CRI = 85 at t_{50}.

As a comparison between previously reported works and this work, a recap table is displayed in Table S2 (Supporting Information).

3. Conclusion

This work provides one of the first examples of hybrid material by insertion of RhB into a blue emissive sustainable and cost-effective and blue-emitting LMOF for photon down-converting coatings applied to blue- and white-emitting HLEDs. The relevance of the blue-emitting **Zn-2-LMOF** lies on its high ϕ values in both powder (50%) and polystyrene (70%) coatings using environmentally friendly moieties (i.e., non rare-earth metal ions) as noted in the prior-art (Cd-based LMOF).[20,18b] This also holds for the white-emitting hybrid **RhB@LMOF** that features an effective energy transfer from the LMOF to the RhB, reaching a white emission band peaking at 480 and 580 nm with a x/y CIE color coordinates of 0.31/0.32 and ϕ of 30–40% in polystyrene coatings. In contrast to OP coatings with RhB, whose emission is quenched by aggregation, the new **Zn-2-LMOF** allows an effective dispersion of the RhB guest acting as a "diluting" agent. Finally, HLEDs with the **Zn-2-LMOF@PS** and the **RhB@LMOF-E@PS** were fabricated as reference and targeted white devices, respectively. Both showed excellent photon down-conversion features, performing blue (x/y CIE color coordinates of 0.28/0.47; 35 lm W^{-1}) and white (x/y CIE color coordinates of 0.31/0.32; CCT of 6835; CRI of 85; 1.4 lm W^{-1}) on-chip HLEDs with stabilities of 20 and 45 h, respectively. The device degradation is attributed to the photoinduced oxidation of **2** that further promotes the photoinduced degradation of RhB.

In view of the above finding, the success of the **Zn-2-LMOF** design lies on i) an twofold increase of ϕ and 1 order of magnitude enhanced photostability of the ligand **2** in OPs and ii) straightforward preparation of white-emitting hybrid in which the RhB is effectively protected. Though these findings have led to average performing blue- and white-emitting HLEDs, we strongly believe that these finding will be instrumental for the design of highly LMOFs for lighting that is still today a barely explored field.

4. Experimental Section

Materials: All the chemicals were purchased from Sigma–Aldrich, Tokyo Chemicals Industry, or Fluorochem without any further purification. The solvents were dried from a solvent purification system MB SPS-800/7 from MBraun, using argon as inert gas and a double column solvent filtration system. Deuterated solvents were bought from Eurisotop or Sigma–Aldrich and used without any further purification. When inert atmosphere was used (i.e., nitrogen or argon), it is specified in the reaction details.

Synthesis: The general procedures are provided as follows, while details about the characterization of the products is provided in the Supporting Information (cf. Scheme 1, Figures S1–S4, Supporting Information).

Synthesis of the MOF Ligand: 1,1,2,2-tetrakis(4-bromophenyl) ethene (**1**) was synthesized according to a previous work.[23] 1,1,2,2-tetraphenylethene (2.5 g; 7.53 mmol, 1 eq.) was put in a watch glass, and the latter was put on the rack of a desiccator. Liquid bromine

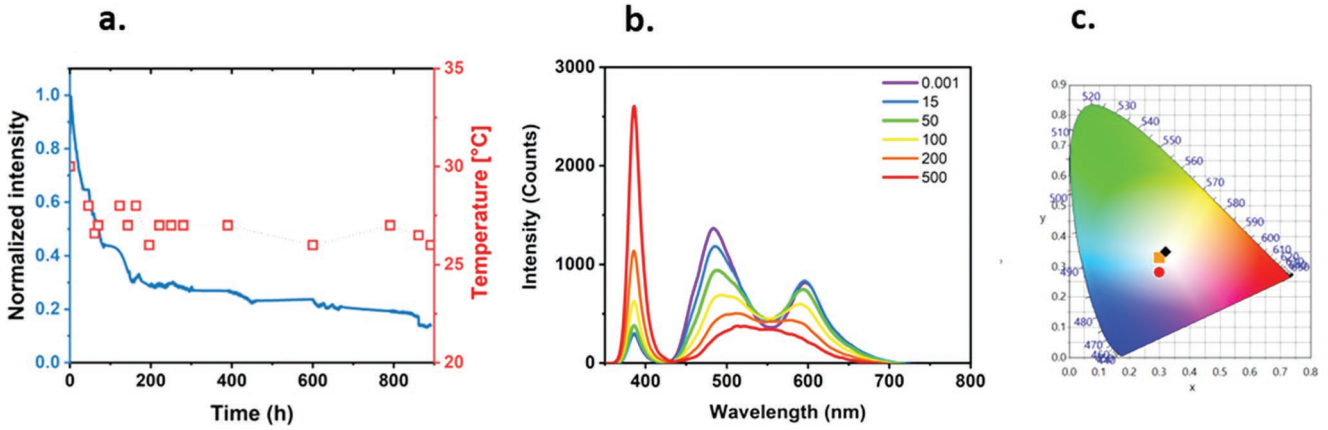

Figure 6. a) Emission intensity and temperature changes of the coatings of remote hybrid light-emitting diode (HLED) with **RhB@LMOF-E@PS** at 50 mA. b) Electroluminescent spectra over time (caption: time given in hours) of remote HLED with **RhB@LMOF-E@PS**. c) x/y CIE color coordinates of the remote HLED with **RhB@LMOF-E@PS** at constant 50 mA under ambient conditions.

(3 ml; 58.5 mmol, 7.8 eq.) was placed onto the bottom of that desiccator. The desiccator was left slightly open, and the reaction was left for 1 week in ambient atmosphere. The dark yellow solid that was obtained was recrystallized in methanol and washed two times with 20 mL of cold methanol to yield the final compound as an off-white powder (4.27 g, yield: 87%).^{1}H NMR (400 MHz, CD_2Cl_2) δ: 7.22 (m, 8H), 6.80 (m, 8H).^{13}C NMR (100 MHz, CD_2Cl_2) δ: 142.0, 140.1, 133.2, 131.6, 121.5, 53.8. HRMS (ESI+): *m/z* calcd. for $C_{26}H_{16}Br_4$ 647.7947, found 647.7938 $[M]^+$.

The synthesis procedure for 1,1,2,2-tetrakis(4-(pyridin-4-yl)phenyl) ethane (**2**) is modified according to a previous work.[26] 1,1,2,2-tetrakis(4-bromophenyl)ethene (**1**) (0.9 g, 1.4 mmol, 1 eq.), pyridine-4-boronic acid (1.025 g, 8.14 mmol, 6 eq.), palladium (II) acetate (104.1 mg, 0.46 mmol, 0.33 eq.), and potassium carbonate (1.31 g, 9.48 mmol, 7 eq.) were put into a 100 mL double neck round-bottom flask. Anhydrous dimethylformamide (DMF, 50 mL) was added and the solution was heated at 150 °C for 48 h under nitrogen. After 48 h, the reaction mixture was cooled down to r.t., and the solvent were removed under vacuum and extracted with dichloromethane (DCM, 3 times 60 mL). The organic layer was collected, washed with water, dried with anhydrous magnesium sulphate, and DCM was evaporated under reduced pressure. The crude product was purified by column chromatography (stationary phase: silica; mobile phase: DCM 94 : 6 methanol) to obtain the pure product as a yellow powder (yield: 573 mg, 64%).^{1}H NMR (400 MHz, CD_2Cl_2) δ: 8.63 (m, 8H), 7.49 (m, 8H), 7.47 (m, 8H), 7.2;2^{13}C NMR (100 MHz, CD_2Cl_2) δ: 142.0, 140.1, 133.2, 131.6, 121.5, 53.8. HRMS (ESI+): *m/z* calcd. for $C_{26}H_{16}Br_4$: 640.2627, found: 641.2683 $[M+H]^+$.

Synthesis of Luminescent MOF: **Zn-2-LMOF** was synthesized according to a solvothermal reaction of $ZnCl_2$ and ligand **2**. In a pressure tube, $ZnCl_2$ (100 mg, 0.73 mmol, 1 eq.) ligand **2** (470 mg, 0.73 mmol, 1eq.), acetic acid (0.5 mL), and DMF (25 mL) were mixed together. The tube was sonicated for 2 min, and was heated in an oil bath at 150 °C for 48 h. The crystalline yellow-greenish crystalline powder was purified by a Soxhlet extraction in ethanol for 24 h. The powder was dried under vacuum in order to obtain the final material.

Synthesis of Luminescent Hybrid MOFs: **Zn-2-LMOF** (10 mg) and RhB were mixed together at different ratios in acetonitrile at 60 °C for 24 h. The amount of RhB involved in the guest insertion process was chosen as followed: 1 mg for the 10% sample (**RhB@LMOF-A**), 2 mg for the 20% sample (**RhB@LMOF-B**), 4 mg for the 40% sample(**RhB@LMOF-C**), 5 mg for the 50% sample (**RhB@LMOF-D**), 10 mg for the 100% (**RhB@LMOF-E**) sample, and 20 mg for the 200% sample (**RhB@LMOF-F**). After 24 h, the suspensions were allowed to cool down to room temperature (r.t.), prior to transferring into centrifuge tubes. The different samples were purified by washing and centrifuging up to 10 times, using hexan-1-ol as a washing solvent. After 10 washing cycles, the supernatant was not colorful anymore, meaning that all the RhB molecules left are inside the MOF's pores. The different samples were dried under vacuum in order to yield the final hybrid materials.

Characterization Techniques: NMR spectra were recorder from a JEOL 400 MHz Year Hold Super Conducting Magnet (400JJYH, JEOL, Tokyo, Japan). Each spectrum was calibrated according to the residual peak of the solvent as internal standard. Liquid-chromatography coupled with HRMS (HPLC-HRMS) was performed in positive mode using a Thermo Fisher Ultimate3000 with Scientific Vanquish Flex UHPLC and a Thermo Fisher Orbitrap (Exactive Plus with Extend Mass Range: Source HESI II). The detector was a Vanquish PDA Detector (VF-XX, detection ≤ 5 ppm). Direct injection HRMS was used using as eluant HPLC grade acetonitrile. PXRD data used in this work were obtained from a Miniflex diffractometer (Rigaku, Tokyo, Japan) with a copper source (1.54Å) and a silicon strip detector (D/teX Ultra, Rigaku), a goniometer radius of 150 mm; both Soller slits at 2.5°; a divergence slit fixed at 0.625°; an anti-scatter slit of 8 mm; and a kβ filter of 0.06 mm nickel foil. The powder was placed on a low background silicon wafer sample holder (cut 911). SEM images were recorded using a DSM 940A (Zeiss, Germany). The sample holders were mounted by sticking a double-sided adhesive tape on an aluminum stub on one side, and a glass disk plate on the other side. The samples were prepared by drop-casting a suspension of the material in ethanol on the glass plate and left at ambient conditions until the complete evaporation of ethanol. The samples were then sputter-coated with gold. SEM images were obtained using 25 keV electron energy, using the secondary electron detector. Thermogravimetric analyses were carried out with a PT1600 analyzer (Linseis, Germany) under ambient atmosphere (TGA, PT1600 Linseis, Selb, Germany) and a heating rate of 10 K min^{-1}. For this purpose, the TG detector was mounted. Each measurement was related to the original sample mass, established at 100%. Nitrogen adsorption–desorption curves were recorded from samples degassed overnight at 80 °C, and corrected for the corresponding blank measurements (Surfer Nano, Thermo Fisher, Waltham, USA). From these, the specific surfaces of the materials were determined by the method of Brunauer, Emmett, and Teller from the relative pressure range $0.05 < P/P0 < 1$.[23] Pore size distributions were recorded in the range 1 nm < *d* <20 nm and were obtained by the method of Broekhoff and de Boer,[24] based on the theory of Barrett, Joyner, and Halenda.[25] UV–Vis experiments were conducted using a UV–NIR spectrophotometer 3600i, Shimadzu, Japan. All the samples were diluted with exactly the same amount of methanol prior to measurement. Solid-state emission and excitation spectra were recorded with an FS5 spectrofluorometer (Edinburgh Instruments) and a Xe lamp as a light source. The powder samples were inserted into a quartz tube, and the latter was placed into a quartz cuvette. The measurements were performed using the cuvette holder (SC-05 sample chamber). Regarding films into polymeric matrixes samples, they were performed in the same way, but the films were directly placed in a quartz cuvette. Solid state excited-state lifetime data were recorded using the same spectrofluorometer and the same sample holder. The light source employed for exciting the sample is a pulsed LED EPLED at 375 nm. Photoluminescence quantum yields were determined using the same spectrofluorometer (FS5, Edinburgh Instruments) together with the integrating sphere setup (SC-30 cuvette holder).

Device Preparation and Characterization: The photon down-converting coatings were prepared and optimized as followed. A 200 mg mL^{-1} polystyrene (PS, average Mw = 350 000 g mol^{-1})[26] solution in toluene was made by mixing 4 g of PS in 20 mL toluene, prior to heating at 80 °C and stirring for 2 h. An amount of 6 mg of the fluorescent material, **Zn-2-LMOF** alone or **RhB@LMOF**, was put in a vial and 900 µL of the PS solution was poured in the vial. The resulting suspension was heated at 80 °C and stirred at 300 rpm for 30 min. The final suspension was allowed to cool down to r.t., and 300 µL of it were put in a well-shaped Teflon mould. The suspension was left to dry for 48 h at r.t., and the resulting dry, dome-shaped coating was recovered. The thickness of the coating was measured using a Helios–Preisser electronic outside micrometre (thickness found: 1.49 ± 0.05 mm). Photostability and conversion measurements were performed as followed: the prepared coatings were placed according to either an on-chip (zero distance to the emitting chip) or a remote (2 cm distance to the emitting chip) configuration on a 380 nm LED (Future Eden 1 W). Luminous efficiency was determined at different applied currents (10–200 mA), while device stability was monitored at constant 50 mA under ambient conditions. The employed power source was a Keithley 2231-A-30-3. The electroluminescence spectra were recorded by an Avantes 2048L spectrometer (300 VA grating, 200 µm slit, CCD detector) coupled with an AvaSphere 30-Irrad integrated sphere. The temperature of the polymer coatings under operation condition was monitored using a thermographic camera FLIR ETS320.

Supporting Information

Supporting Information is available from the Wiley Online Library or from the author.

Acknowledgements

The authors gratefully thank Dr. Jean-Louis Schmitt and Hava Aksoy for the HR–MS experiments. R.D.C. acknowledges the European

Union's Horizon 2020 research and innovation FET-OPEN under grant agreement ARTIBLED No. 863170, the ERC-Co InOutBioLight No. 816856. R.D.C. and Y.A. acknowledge the European Union's Horizon 2020 research and innovation CuMOF-LED No. 896800.

Open access funding enabled and organized by Projekt DEAL.

Conflict of Interest

The authors declare no conflict of interest.

Data Availability Statement

The data that support the findings of this study are available from the corresponding author upon reasonable request.

Keywords

blue-emitting metal organic framework, hybrid light-emitting diodes, luminescent metal organic framework, photon down-converting coatings, white-emitting host:guest hybrid material

Received: November 14, 2022
Published online: December 18, 2022

[1] a) S. Ye, F. Xiao, Y. X. Pan, Y. Y. Ma, Q. Y. Zhang, *Mater. Sci. Eng., R* **2010**, *71*, 1; b) J. McKittrick, L. E. Shea-Rohwer, *J. Am. Ceram. Soc.* **2014**, *97*, 1327.

[2] a) O. Kotova, S. Comby, C. Lincheneau, T. Gunnlaugsson, *Chem. Sci.* **2017**, *8*, 3419; b) Z. Sun, F. Bai, H. Wu, D. M. Boye, H. Fan, *Chem. Mater.* **2012**, *24*, 3415; c) Y. Wang, G. Zhu, S. Xin, Q. Wang, Y. Li, Q. Wu, C. Wang, X. Wang, X. Ding, W. Geng, *J. Rare Earths* **2015**, *33*, 1.

[3] a) Y. Cho, S. Pak, B. Li, B. Hou, S. Cha, *Adv. Funct. Mater.* **2021**, *31*, 2104239; b) J.-H. Kim, D.-Y. Jo, K.-H. Lee, E.-P. Jang, C.-Y. Han, J.-H. Jo, H. Yang, *Adv. Mater.* **2016**, *28*, 5093.

[4] a) V. Fernández-Luna, P. B. Coto, R. D. Costa, *Angew. Chem., Int. Ed.* **2018**, *57*, 8826; b) E. Fresta, V. Fernández-Luna, P. B. Coto, R. D. Costa, *Adv. Funct. Mater.* **2018**, *28*, 1707011. c) M. D. Weber, L. Niklaus, M. Pröschel, P. B. Coto, U. Sonnewald, R. D. Costa, *Adv. Mater.* **2015**, *27*, 5493.

[5] Y. Hu, X. Liang, D. Wu, B. Yu, Y. Wang, Y. Mi, Z. Cao, Z. Zhao, *J. Mater. Chem.* **2020**, *8*, 734.

[6] P. Coppo, M. Duati, V. N. Kozhevnikov, J. W. Hofstraat, L. De Cola, *Angew. Chem., Int. Ed.* **2005**, *44*, 1806.

[7] N. Muhamad Sarih, P. Myers, A. Slater, B. Slater, Z. Abdullah, H. A. Tajuddin, S. Maher, *Sci. Rep.* **2019**, *9*, 11834.

[8] J. He, S. Yang, K. Zheng, Y. Zhang, J. Song, J. Qu, *Green Chem.* **2018**, *20*, 3557.

[9] a) C. Ezquerro, E. Fresta, E. Serrano, E. Lalinde, J. García-Martínez, J. R. Berenguer, R. D. Costa, *Mater. Horiz.* **2019**, *6*, 130. b) L. Niklaus, H. Dakhil, M. Kostrzewa, P. B. Coto, U. Sonnewald, A. Wierschem, R. D. Costa, *Mater. Horiz.* **2016**, *3*, 340.

[10] A. Espasa, M. Lang, C. F. Aguiño, D. Sanchez-deAlcazar, J. P. Fernández-Blázquez, U. Sonnewald, A. L. Cortajarena, P. B. Coto, R. D. Costa, *Nat. Commun.* **2020**, *11*, 879.

[11] a) K. Zhang, J. Liu, Y. Zhang, J. Fan, C.-K. Wang, L. Lin, *J. Phys. Chem. C* **2019**, *123*, 24705; b) Y. Huang, J. Xing, Q. Gong, L.-C. Chen, G. Liu, C. Yao, Z. Wang, H.-L. Zhang, Z. Chen, Q. Zhang, *Nat. Commun.* **2019**, *10*, 169.

[12] a) S. Wang, D. Wu, S. Yang, H. Zhen, Z. Lin, Q. Ling, *J. Mater. Chem. C* **2020**, *8*, 12623; b) D. Yao, S. Xu, Y. Wang, H. Li, *Mater. Chem. Front.* **2019**, *3*, 1080; c) Y. Tang, H. Wu, W. Cao, Y. Cui, G. Qian, *Adv. Opt. Mater.* **2021**, *9*, 2001817; d) G. A. Leith, C. R. Martin, J. M. Mayers, P. Kittikhunnatham, R. W. Larsen, N. B. Shustova, *Chem. Soc. Rev.* **2021**, *50*, 4382.

[13] a) N. L. Rosi, J. Eckert, M. Eddaoudi, D. T. Vodak, J. Kim, M. O'Keeffe, O. M. Yaghi, *Science* **2003**, *300*, 1127; b) J. L. C. Rowsell, O. M. Yaghi, *Microporous Mesoporous Mater.* **2004**, *73*, 3; c) H.-C. Zhou, J. R. Long, O. M. Yaghi, *Chem. Rev.* **2012**, *112*, 673.

[14] a) H. Li, K. Wang, Y. Sun, C. T. Lollar, J. Li, H.-C. Zhou, *Mater. Today* **2018**, *21*, 108; b) Li, H.-M. Wen, W. Zhou, B. Chen, *J. Phys. Chem. Lett.* **2014**, *5*, 3468; c) Q. Qian, P. A. Asinger, M. J. Lee, G. Han, K. Mizrahi Rodriguez, S. Lin, F. M. Benedetti, A. X. Wu, W. S. Chi, Z. P. Smith, *Chem. Rev.* **2020**, *120*, 8161; d) Z. Kang, L. Fan, D. Sun, *J. Mater. Chem. A* **2017**, *5*, 10073.

[15] a) J. A. Mason, M. Veenstra, J. R. Long, *Chem. Sci.* **2014**, *5*, 32; b) S. Ma, H.-C. Zhou, *Chem. Commun.* **2010**, *46*, 44,. c) J. Ren, H. W. Langmi, B. C. North, M. Mathe, *Int. J. Energy Res.* **2015**, *39*, 607.

[16] a) V. Pascanu, G. González Miera, A. K. Inge, B. Martín-Matute, *J. Am. Chem. Soc.* **2019**, *141*, 7223; b) Y.-S. Wei, M. Zhang, R. Zou, Q. Xu, *Chem. Rev.* **2020**, *120*, 12089; c) P. García-García, M. Müller, A. Corma, *Chem. Sci.* **2014**, *5*, 2979; d) P. Kittikhunnatham, G. A. Leith, A. Mathur, J. K. Naglic, C. R. Martin, K. C. Park, K. McCullough, H. D. A. Chathumal Jayaweera, R. E. Corkill, J. Lauterbach, S. G. Karakalos, M. D. Smith, S. Garashchuk, D. A. Chen, N. B. Shustova, *Angew. Chem., Int. Ed.* **2022**, *61*, e202113909.

[17] a) P. Horcajada, R. Gref, T. Baati, P. K. Allan, G. Maurin, P. Couvreur, G. Férey, R. E. Morris, C. Serre, *Chem. Rev.* **2012**, *112*, 1232; b) R. F. Mendes, F. Figueira, J. P. Leite, L. Gales, F. A. A. Paz, *Chem. Soc. Rev.* **2020**, *49*, 9121; c) L. Cooper, T. Hidalgo, M. Gorman, T. Lozano-Fernández, R. Simón-Vázquez, C. Olivier, N. Guillou, C. Serre, C. Martineau, F. Taulelle, D. Damasceno-Borges, G. Maurin, Á. González-Fernández, P. Horcajada, T. Devic, *Chem. Commun.* **2015**, *51*, 5848; d) R. C. Alves, Z. M. Schulte, M. T. Luiz, P. Bento da Silva, R. C. G. Frem, N. L. Rosi, M. Chorilli, *Inorg. Chem.* **2021**, *60*, 11739.

[18] C.-Y. Sun, X.-L. Wang, X. Zhang, C. Qin, P. Li, Z.-M. Su, D.-X. Zhu, G.-G. Shan, K.-Z. Shao, H. Wu, J. Li, *Nat. Commun.* **2013**, *4*, 2717.

[19] a) T. Mondal, S. Bose, A. Husain, U. K. Ghorai, S. K. Saha, *Opt. Mater.* **2020**, *100*, 109706; b) D. Micheroni, Z. Lin, Y.-S. Chen, W. Lin, *Inorg. Chem.* **2019**, *555*, 10669; c) Y. Yang, W. Li, C. Sun, G. Shan, C. Qin, K. Shao, J. Wang, Z. Su, *Adv. Opt. Mater.* **2022**, *10*, 2200174; d) Y. Cui, T. Song, J. Yu, Y. Yang, Z. Wang, G. Qian, *Adv. Funct. Mater.* **2015**, *25*, 4796; e) Q. Yan, B. Li, W. Jiang, G. Yong, *Opt. Mater.* **2020**, *109*, 110449.

[20] a) Y. Z. J.-C. Tan, *iScience* **2021**, *24*, 103035; b) J. Yuan, G. Feng, J. Dong, S. Lei, W. Hu, *Nanoscale* **2021**, *13*, 12466.

[21] X.-L. Hu, C. Qin, X.-L. Wang, K.-Z. Shao, Z.-M. Su, *Chem. Commun.* **2015**, *51*, 17521.

[22] a) W. Li, J. Wang, M. Tebyetekerwa, Y. Ding, Z. Qiu, C. Yan, F. Liu, J. Zhang, *Adv. Powder Technol.* **2019**, *30*, 2218; b) W. Li, J. Wang, Y. Xie, M. Tebyetekerwa, Z. Qiu, J. Tang, S. Yang, M. Zhu, Z. Xu, *Prog. Org. Coat.* **2018**, *120*, 1.

[23] S. Brunauer, P. H. Emmett, E. Teller, *J. Am. Chem. Soc.* **1938**, *60*, 309.

[24] J. C. P. Brohekoff, J. H. De Boer, *J. Catal.* **1967**, *9*, 8.

[25] E. P. Barrett, L. G. Joyner, P. P. Halenda, *J. Am. Chem. Soc.* **1951**, *73*, 373.

[26] a) T. Guner, E. Aksoy, M. M. Demir, C. Varlikli, *Dyes Pigm.* **2019**, *160*, 501; b) M. Mosca, R. Macaluso, I. Crupi, in *Polymers for Light-Emitting Devices and Displays* (Eds: Inamuddin, R. Boddula,

M. I. Ahamed, A. M. Asiri), Wiley, Weinheim **2020**; c) E. Kozma, W. Mróz, F. G. , *Dyes Pigm.* **2015**, *114*, 138.
[27] Q. Gong, Z. Hu, B. J. Deibert, T. J. Emge, S. J. Teat, D. Banerjee, B. Mussman, N. D. Rudd, J. Li, *J. Am. Chem. Soc.* **2014**, *136*, 16724.
[28] N. B. Shustova, B. D. McCarthy, M. Dinča, *J. Am. Chem. Soc.* **2011**, *133*, 20126.
[29] Z. Wei, Z.-Y. Gu, R. K. Arvapally, Y.-P. Chen, R. N. McDougald Jr., J. F. Ivy, A. A. Yakovenko, D. Feng, M. A. Omary, H.-C. Zhou, *J. Am. Chem. Soc.* **2014**, *136*, 8269.
[30] W. Li, J. Wang, Y. Xie, M. Tebyetekerwa, Z. Qiu, J. Tang, S. Yang, M. Zhu, Z. Xu, *Prog. Org. Coat.* **2018**, *120*, 1.
[31] M. Pauchard, A. Devaux, G. Calzaferri, *Chem. - Eur. J.* **2000**, *6*, 3456.
[32] J. M. Dixon, M. Taniguchi, J. S. Lindsey, *Photochem. Photobiol.* **2005**, *81*, 212.
[33] a) Y. Atoini, E. A. Prasetyanto, P. Chen, D. Jonckheere, D. De Vos, L. De Cola, *Supramol. Chem.* **2017**, *29*, 758; b) T. Dhawa, S. Chattopadhyay, G. De, S. Mahanty, *ACS Omega* **2017**, *2*, 6481.
[34] M. A. Elsayed, *Orbital: Electron. J. Chem.* **2014**, *6*, 195.